High-throughput transcriptomic evaluation of per- and polyfluoroalkyl substances (PFAS) in primary human liver spheroids to inform read-across

A. Rowan-Carroll[1], A. Reardon[1], K. Leingartner[1], R. Gagné[1] , A. Williams[1], B. Kuo [1], J. Bourdon-Lacombe[2], I. Moffat[2], R.Carrier[2], A. Nong[1], L. Lorusso[3], S.S. Ferguson[4], E. Atlas[1 *], C. Yauk[5,1*]
[1]Environmental Health Science and Research Bureau, Healthy Environments and Consumer Safety Branch (HECSB), Health Canada, [2] Water and Air Quality Bureau, HECSB, Health Canada, [3] Chemicals and Environmental Health Management Bureau, HECSB, Health Canada, [4] US National Institute of Environmental Health Sciences, [5]Dept. of Biology, University of Ottawa.

For submission to Toxicological Sciences

* To Whom correspondence should be addressed: carole.yauk@uottawa.ca, carole.yauk@canada.ca and ella.atlas@canada.ca

Keywords: TempO-Seq, PFAS, Liver spheroids, benchmark concentration, new approach methodology, bioactivity exposure ratio

The following secure token has been created to allow review of record GSE144775 while it remains in private status: wlqxagaadnmjxmn.

Abstract (250word limit)

Per- and poly-fluoroalkyl substances (PFAS) are widely found in the environment because of their extensive use and persistence. Although a few PFAS are well studied, most lack toxicity data to inform human health hazard and risk assessment. This study focussed on four model PFAS: perfluorooctanoic acid (PFOA; 8 carbon), perfluorobutane sulfonate (PFBS; 4 carbon), perfluorooctane sulfonate (PFOS; 8 carbon), and perfluorodecane sulfonate (PFDS; 10 carbon). Human primary liver cell spheroids (i.e., pooled-donor) were exposed to 10 concentrations of PFAS over four time-points. The approach aimed to: (1) identify the extent to which the PFAS modulated gene expression; (2) identify similarities in biological responses; (3) compare PFAS potency through benchmark concentration (BMC) analysis; and (4) derive bioactivity exposure ratios (BERs: ratio of concentration at which biological response occurs converted to administered equivalent dose relative to human daily exposure). All PFAS induced transcriptional changes of cholesterol biosynthesis and lipid metabolism, and appeared to activate PPARα. PFOS exhibited the most transcriptional perturbations and had a highly similar gene expression profile to PFDS. PFBS induced the least transcriptional changes and had the highest BMCs. The data indicate that these four chemicals may have common molecular targets and toxicities, but that PFOS and PFDS are the most similar. BERs derived for PFOA and PFOS had relatively low margins; the transcriptomic BER was slightly more conservative than BERs derived from rodent apical endpoints used as points of departure in risk assessment. The data provide a baseline on which to compare the toxicity of other PFAS using this testing strategy.

Introduction (750word limit)

Per- and poly-fluoroalkyl substances (PFAS) are a class of chemicals ubiquitously found in the environment. Their unique hydrophobic and lipophobic properties has led to their use in many consumer products and their persistence, and bioaccumulation potential have led to their detection in wildlife and humans worldwide (Armitage *et al.*, 2006; Wania, 2007; Schenker *et al.*, 2008; Stemmler and Lammel, 2010; Armitage *et al.*, 2009a, 2009b). Although perfluorooctane sulfonate (PFOS) and perfluorooctanoate (PFOA) have been retired from North American production, they continue to be found in drinking water and contaminated sites within Canada (Paul and Auer, 2000; Canada. Health Canada., 2017; Shi *et al.*, 2015; Z. Wang *et al.*, 2014; Wang *et al.*, 2016; Liu *et al.*, 2017). Moreover, there are thousands of PFAS that remain in production globally, with little toxicological data available for the vast majority of them (Linda S. Birnbaum, 2018).

The adverse health effects of PFOS and PFOA in humans are well documented, including increased cholesterol levels (Eriksen *et al.*, 2013; Geiger *et al.*, 2014), decreased human fertility (Bach *et al.*, 2016), and reduced immune response (National Toxicology Program NTP NTP Monograph Immunotoxicity Associated with Exposure to Perfluorooctanoic Acid or Perfluorooctane Sulfonate, 2016; Kielsen *et al.*, 2016; Health Canada, 2018b). Recently the US Environmental Protection Agency has recognized the need for, and developed an action plan to address concerns of PFAS in drinking water, reduction of exposure, safety in commerce and support for communications (United States Environmental Protection Agency, 2020).

The effects of several PFAS have been extensively studied in animal models. For example, wild-type and PPARα-null mice treated with perfluorooctanoic acid (PFOA), perfluorononanoic acid (PFNA), or perfluorohexane sulfonate (PFHxS) exhibit steatosis, which is characterised by an accumulation of lipids in hepatocytes (Das *et al.*, 2017). The accumulation of fatty acids ultimately leads to liver disease and liver failure (Das *et al.*, 2017). Studies conducted in rodents have also shown that PFOS and PFOA exposure can lead to cancer (Health Canada, 2018b; Filgo *et al.*, 2015; Biegel *et al.*, 2001; Butenhoff *et al.*, 2012). Conversely, a critical review of the human literature found

no causal association between cancer in humans and exposure to PFOA and PFOS (Chang *et al.*, 2014). As such, the liver has been identified as the critical epidemiological endpoint in Health Canada's existing regulatory guidelines on PFAS (Health Canada, 2018b).

Acquiring information on data-poor substances for risk assessment has been a challenge for regulatory agencies worldwide given the cost and time required to conduct traditional toxicological research. To accelerate the pace of chemical risk assessments, global efforts have focused on increasing the use of New Approach Methodologies (NAMS) (Kavlock *et al.*, 2018; Krewski *et al.*, 2020). *In silico* predictions, high throughput screening, novel *in vitro* models, *in vitro* to *in vivo* extrapolation (IVIVE), and read-across are some of the NAMs with increasing use in risk assessment for chemicals with limited data. High-throughput transcriptomics, when paired with physiologically-relevant model systems, is a particularly powerful methodology to obtain information about the broad scope of biological perturbations that result from chemical exposures. New technologies now enable gene expression analyses directly from cell lysates, which significantly increases the ease and speed with which transcriptomic data can be produced (Trejo *et al.*, 2019).

To address the need for efficient assessment of data-poor PFAS, we sought to develop an approach to broadly screen for PFAS-induced biological perturbations through global gene expression profiling of human primary cell liver spheroids. A main objective was to establish baseline transcriptomic profiles and an analytical pipeline for future evaluations of data-poor PFAS. Liver spheroids were exposed to nine concentrations of PFAS and sampled at four time points. To establish our approach, we focused on four prototype PFAS: PFOS (8 carbon), PFOA (8 carbon), perfluorodecane sulfonate (PFDS: long chain, 10 carbon), and perfluorobutane sulfonate (PFBS: short chain, 4 carbon). Microscopy was used to evaluate phenotypic changes in the spheroids, and the lactose dehydrogenase activity assay was used to assess cytotoxicity over time. The TempO-Seq platform using the NIEHS S1500 gene set (https://federalregister.gov/a/2015-08529) was applied for transcriptomic analysis. PFAS were compared based on the induction of differentially expressed genes (DEGs),

hierarchical clustering and principle component analysis (PCA), pathway and upstream regulator enrichment, and transcriptomic benchmark concentrations (BMCs). Bioactivity-exposure ratios (BERs) for PFOS and PFOA were calculated by comparing human administered equivalent dose (AED: the daily dose required to achieve the *in vitro* concentration of interest) to human exposure levels. A small BER suggests that biological perturbations occur at concentration that approach external human exposure levels. This initial research project was used to inform experimental design and analytical approach for analysis of a second larger group of data-poor PFAS (Reardon *et al*., 2020 sister paper).

Methods

Chemicals and preparation of working solutions

PFOS (95% purity CAS 1763-23-1), PFOA (95% purity CAS 335-67-1), PFBS (95% purity CAS 375-73-5) and Cyclosporine A (CsA) were purchased from Sigma-Aldrich (Oakville, ON) and PFDS was purchased from Toronto Research Chemicals (95% purity CAS 335-77-3 Toronto, ON). Chemicals were dissolved in dimethylsulfoxide (DMSO, Sigma-Aldrich, Oakville, ON) to prepare working stock solutions ranging in concentration from 0.02 to 30 mM. Each PFAS compound was tested at 10 different concentrations (0 to 100 µM), in quadruplicate experiments. For microscopic characterization, a 30 mM working stock of CsA in DMSO was prepared. The final concentration of DMSO in the media ranged between 0.1%-0.3%. Concentrations of DMSO in media varied for two working concentrations only, 50 and 100 µM. A standard 0.1% DMSO was used for working concentrations of PFAS (0.02 -25 µM), 0.17% DMSO was used for 50 µM PFAS and 0.3% DMSO was used for the100 µM. The percent of DMSO varied as the top chemical stocks were all kept at a concentration of 30 µM for all PFAS due to solubility. All experimental concentrations of PFAS were matched to vehicle only (DMSO) controls at the same concentration, i.e., PFAS at a working concentration of 100 µM (0.3% DMSO) was matched to 0.3% DMSO controls.

Cell Culture

3D InSight™ Human Liver Microtissues were purchased from InSphero (Brunswick, ME) in a 96 well format, with a single spheroid per well. These spheroids are a co-culture model from 10 different human liver donors and are a metabolically active system of hepatocytes and Kupffer cells. Upon arrival, the media were replaced with serum free cell medium (InSphero Human Liver Maintenance Medium–Tox) and spheroids were allowed to acclimate for 24 hours prior to PFAS exposures.

Liver spheroids were cultured under sterile conditions with incubation at 37°C, 5% CO_2. Liver spheroids were exposed for 1, 4, 10 or 14 days to PFOS, PFOA, PFDS, PFBS or DMSO control diluted in culture medium. Final treatment doses were 0.02, 0.1, 0.2, 1, 2, 10, 20, 50 and 100uM of each of the 4 PFAS chemicals.

The highest concentration tested was 100 µM, as per the US EPA's Toxcast program. Although the top concentration is high, it is useful to have a top concentration yielding a robust transcriptomic response for BMD modeling and provides important context analogous to LD_{50} for guideline toxicology studies. From there, we scaled down in approximate half-log concentrations. Media were replaced every 3 days with freshly diluted chemical, and spent media were reserved for cytotoxicity analysis. Spheroids designated for microscopy were treated with 0.1% DMSO, then, 48 hours prior to the Day-14 time point, half of them were dosed with 30 uM CsA for immunostaining. Spheroids designated for TempO-Seq library building and sequencing were washed with Dulbecco's phosphate-buffered saline (DPBS; Thermo Fisher Scientific Waltham, MA) and lysed using 5-7 µl of TempO-Seq lysis buffer (BioSpyder Technologies Inc Carlsbad, CA). Liver spheroids were triturated and allowed to complete lysis for approximately 10 minutes before freezing at -80^{0}C. Spheroids reserved for sequencing analysis were collected at 24 hr, Day-4, Day-10, and Day-14 time points.

Cytotoxicity Assessment

Cytotoxicity was measured from spent culture media collected every 3 days during media replenishment using the lactate dehydrogenase assay (LDH-Glo Cytotoxicity AssayPromega Corp Madison, USA). Media was diluted 1:10 in storage buffer (200 mM Tris-HCl, pH 7.3, containing 10% glycerol and 1% bovine serum albumin) and kept frozen at -80°C until analysis. For the assay, thawed samples were

diluted with an equal volume of LDH Detection Reagent and equilibrated for 60 minutes at room temperature before reading the luminescence (GloMax 96 Microplate Luminometer, Promega Corp Madison, WI USA) in relative luminescence units (RLU). Treatment effects on cytotoxicity were determined after performing statistical analysis of the RLU data after blank subtraction in Sigma Plot 13™, using the Kruskal-Wallis one-way analysis of variance on ranks, followed by the Dunn's multiple comparison versus the control group for each timepoint, with N=4 except Day 14 (N=2). The sample RLU was converted to a ratio by division with the average RLU of the DMSO controls and the mean and standard deviations of these ratios were calculated for each treatment and time point.

Microscopy

Spheroid whole mounts were prepared on Day-4 and Day-14 according to a protocol provided by InSphero Inc. (Technical Protocol 008 c. 2015), with modifications. Briefly, spheroids were fixed with 4% paraformaldehyde in phosphate buffered saline (PBS) for 1 hour, permeabilized with 0.2% Triton-X100 in PBS for 30 minutes, and blocked with 5% bovine serum albumin in PBS for 1 hour at room temperature. To identify Kupffer cells, on Day-4, spheroids were incubated with CD-68 antibody (1:100; Santa Cruz CD68 (E-11): sc-17832 conjugated to AlexaFluor 594) overnight at 4°C, then incubated with 1:40 phalloidin (Life Technologies 12379 conjugated to AlexaFluor 488 Carlsbad, CA) and DAPI (2 ug/ml; Sigma D8417 Oakville, ON) in PBS for 45 minutes at room temperature.

On Day-14, spheroids were divided into two groups. Some spheroids were incubated with CYP3A4 primary antibody (1:00; Santa Cruz CYP3A4 (HL3): sc-53850 conjugated to AlexaFluor 647 Dallas, TX) overnight at 4°C, then stained with phalloidin and DAPI in PBS for 45 minutes at room temperature. The second group of spheroids were incubated with Nile Red (1 µg/ml; Sigma 19123 Oakville, ON) and DAPI (2 µg/ml; Sigma D8417 Oakville, ON) in PBS for 30 minutes at room temperature. After antibody incubation and three washes with PBS, spheroids were transferred to glass microscope slides, mounted with Prolong Gold Mounting Medium (Invitrogen P36934, Burlington,

ON), and coverslipped. Confocal laser-scanning immunofluorescence microscopy was performed using a Leica TCS SP8 microscope.

TempO-Seq Library Building and Next Generation Sequencing

Gene expression was measured using the human TempO-Seq S1500 panel (BioSpyder Technologies Inc. Carlsbad, CA). This targeted RNA-seq panel is comprised of 3000 genes selected by the NIEHS to represent a biologically diverse set of pathways that are toxicologically responsive (https://federalregister.gov/a/2015-08529). For TempO-Seq analysis, liver spheroids were exposed to nine concentrations of the four PFAS and solvent control (DMSO), over the four time points (1, 4, 10, and 14 days). Spheroids were lysed *in situ* using 2 x TempO-Seq lysis buffer diluted with an equal amount of PBS. Lysates and positive controls (Human Universal Reference RNA - uhrRNA (Agilent Cat# 740000, Santa Clara, California), and Human Brain Total RNA brRNA (ThermoFisher AM7962, Waltham, Massachusetts), as well as no-cell negative controls (1X TempO-Seq lysis buffer alone) were hybridized to the detector oligo mix following the manufacturer's instructions (TEMPO-SEQ Human Tox +Surrogate with Standard Attenuation Transcriptome Kit (96 Samples) BioSpyder Technologies, Inc. Hybridization was followed by nuclease digestion of excess oligos, detector oligo ligation, and amplification of the product with the tagged primers according to manufacturer's instructions. At the time of amplification, each sample was ligated to a sample-specific bar code that allows for combining samples for sequencing purposes. Labelled amplicons were then pooled and purified using NucleoSpin Gel and PCR Clean-up kits, (Takara Bio USA, Inc. Mountain View, CA). Libraries were sequenced in-house using a NextSeq 500 High-Throughput Sequencing System (Illumina San Diego, California) using 50 cycles from a 75-cycle high throughput flow cell. A median read depth of 2 million reads/sample was achieved.

Data processing and identification of Differentially Expressed Genes (DEGs)

Reads were extracted from the bcl files and demultiplexed (i.e., assigned to respective sample files) with bcl2fastq v. 2.20.0.42. The fastq files were processed with the "pete. star. script_v3.0" supplied by BioSpyder. Briefly, the script uses star v.2.5 to align the reads and the qCount function from QuasR to extract the feature counts specified in a gtf file from the aligned reads.

The data were then passed through internal quality control scripts. Boxplots of the log2 CPM (counts per million) were plotted to ensure a reproducible distribution between replicates within a group. Read counts were also used to identify overtly cytotoxic concentrations alongside LDH assay results. Samples with low read counts were often associated with high levels of cytotoxicity as measured in the LDH assay. Hierarchical clustering plots were generated (hclust function: default linkage function of hclust function in R; complete-linkage) of all the samples per time point using a distance metric defined as 1-Spearman correlation in order to identify potential outliers. Low count probes (i.e. probes that did not have a median of 5 counts in at least one group) were flagged as absent genes and eliminated from the dataset. To account for differences in the percentage of DMSO used, the data were normalized to matched controls and rescaled to the average of the 0.1% DMSO dose group.

DEG analysis was conducted on the counts using the default parameters of DESeq2 v1.24 with respective control and exposure groups. Probes reaching the threshold of a false discovery rate (FDR) adjusted p-value $\leq$ 0.05 and an absolute fold change $\geq$ 1.5 (on a linear scale) were flagged (probes passing filters; PPF) and retained for further analyses.

Benchmark Concentration (BMC) and Post DEG analysis

Best practices as recommended by the US EPA's expert panel on genomic BMD analysis were followed. Heatmaps were generated with the pheatmapfunction from R with both the row and column distances defined as 1-Spearman correlation. Values were averaged between replicates; CPM mean values of PPFs were averaged between replicates within each group. Resulting values were subsequently log2 transformed. The principal components were calculated with the prcompR function. The percentages of variation on the axes were gathered from the “importance” field produced by the summary function applied to the resulting object of the prcomp function. The work above was done with R v.3.6.1. Further details on pipeline analysis are available in Supplemental file 1. PCA plots were generated with averaged PPF values.

Functional analysis using Ingenuity Pathway Analysis

Functional analysis of the DEG list was conducted using Ingenuity Pathway Analysis (IPA, Qiagen, Redwood City, CA, USA) using genes with FDR-corrected p-value $\leq$ 0.05 and absolute fold change $\geq$ 1.5. Right-tailed Fisher's exact tests were used to calculate the probability of enrichment of biological functions, canonical pathways, and upstream regulators. The z-score, a statistical predictor of relationship between a direct observation and a prediction of activation/suppression of a particular pathway, upstream regulator or disease, was set to +/- absolute 2.0, which is considered a significant cut off (Ingenuity Pathway Analysis:https://www.youtube.com/watch?v=ub7GLpD8dPQ, 2017; Joakim Ek *et al.*, 2015).

Benchmark concentration (BMC) – Gene-level analysis

BMC modeling was conducted using BMDExpress v.2.2, a free software package that is available for download (https://github.com/auerbachs/BMDExpress-2/releases). Additional information on BMDExpress is available (https://github.com/auerbachs/BMDExpress-2/wiki/Benchmark-Dose-Analysis). Normalized counts per million with the mapped reads for genes from the TempO-Seq analysis were treated in the same manner as previously described, and overtly cytotoxic samples were removed. Imported data into BMDexpress underwent pre-filtering using the Williams' Trend Test with 100 permutations and a 1.5-fold change (FC) cutoff to select probes (i.e., genes) that exhibit significant monotonically increasing or monotonically decreasing concentration-response ($p < 0.05$). Data exhibiting an increasing or decreasing change in response were modeled using Hill, Power, Linear, Polynomial (2° and 3°), and Exponential (2, 3, 4, 5) models to identify potential concentration-response relationships and best fit. For linear and polynomial models, the Nested Chi-square test was used to determine best-fit models followed by a comparison of Akaike information criterion (AIC) for nested models (Hill and Power) with a goodness of fit p-value of 0.1. Hill models were flagged if the 'k' parameter was less than 1/3 the lowest (non-solvent control) concentration, and in the case of a flagged Hill model, the next best-fit model with a goodness of fit p-value > 0.05 was selected. Additional parameters included a BenchMark Response (BMR) factor of 1 standard deviation (SD)

relative to the response of controls, a confidence level of 0.95, power restricted to ≥ 1, and maximum of 250 iterations, (maximum iterations represent a convergence criterion for the model). Applied filters to best-fit models excluded data with highly uncertain BMCs ($p < 0.1$, BenchMark Concentration Upper threshold/ BenchMark Concentration Lower Threshold ≥ 40) as well as data producing BMC values > the highest non-cytotoxic concentration (e.g., 100 µM). BMC gene accumulation plots reflecting the distribution of gene-level BMCs across the range of concentrations, and gene-level BMC estimates from best-fit models were exported from BMDExpress. A transcriptomic point of departure (POD) was determined from the median BMC of all filtered genes adhering to best-fit models and a bootstrap R-script producing 95 % confidence intervals (median BMC ± 95 % CI).

Derivation of the Bioactivity Exposure Ratio (BER)

Transcriptional BMC values were converted to an AED using a conversion factor derived as described in Wambaugh *et al*. 2013. To derive a BER, AEDs (mg/kg-BW/day) were compared to the upper limit of the daily US population exposure (95th percentile) for PFOA (4.50×10^{-04} mg/kg-BW/day) and PFOS (4.76×10^{-04} mg/kg-BW/day) obtained from the US EPA comptox dashboard (https://comptox.epa.gov/dashboard, accessed: January 2020). The other PFAS within the current investigation (PFBS and PFDS) were excluded from BER calculation due to limited exposure data available for US and Canadian populations. For our purposes, the reverse dosimetry approach (Wetmore *et al.*, 2015a) for PFOA and PFOS (as described in Wambaugh et al. 2013) was used to determine a conversion factor to calculate the AED from the BMC estimate of *in vitro* models (Wambaugh *et al.*, 2013).

Two approaches to BER derivation were used. In **Approach 1**, the BER was calculated using the lower bound 5th percentile AED from the gene-level BMC analysis that was rounded to the nearest gene with an integer of greater than or equal value (i.e., the ceiling) and compared to the population exposure. This methodology has been used in previous work to represent a lower bound estimate of *in vivo* adverse effects within the ToxCast database in order to derive a BER (Paul Friedman *et al.*, 2020). In **Approach 2**, BER was derived based on data demonstrating a strong correlation

between the dose at which apical effects *in vivo* occur and the lowest (most sensitive) *in vivo* pathway BMC (Thomas *et al.*, 2013). The pathway level analysis was conducted using the built-in Defined Category Analysis function within BMDExpress. Pathway-level estimates were derived from genes meeting the criteria of best-fit models mapped to probes from the IPA database (downloaded October 2019). Estimates were removed if they contained promiscuous probes (annotating to more than one gene) or contained genes with a BMC > highest concentration from the category descriptive statistics, BMC with a goodness of fit p-value < 0.1, or a BMCU/BMCL value > 40. Exported pathway level estimates included additional filters limiting probe-sets to pathways with ≥ 3 genes passing all previous filters and with ≥ 5% of pathway genes affected. Each approach was then compared to a reference AED value derived from *in vivo* animal data that were used to determine drinking water guidelines for PFOA (Guidelines for Canadian Drinking Water Quality Guideline Technical Document Perfluorooctanoic Acid (PFOA))and PFOS (Health Canada, 2018b) for the purpose of risk assessment.

Results

Liver Spheroids and Microscopy

In order to assess the composition of the liver spheroid model, approximately 25 spheroids were stained with CD68, a marker of Kupffer cells (Figure 1A). As anticipated, the spheroids stained positive for CD68, confirming the presence of this native cell type that is part of the normal liver composition. The spheroids were likewise treated with a known inducer of liver damage, CsA for 48 hrs, and then processed for microscopic evaluation (Figure 1B). Treatment with 30 µM CsA induced expression of CYP3A4, a member of the cytochrome P450 oxidizing family of enzymes responsible for the oxidation toxicants (Zanger and Schwab, 2013), and increased lipid accumulation as assessed by Nile Red staining. These results confirm that the spheroid hepatocytes were responding as expected.

Cytotoxicity Assessment

The LDH-Glo assay was used to measure cytotoxicity over the course of the experiment. Cytotoxicity was evaluated at every media change (every 3 days).

Exposure of the liver cell spheroids to PFOA, the sole carboxylic acid of the group, did not cause significant cytotoxicity over time at the lower concentrations (0.02 – 20 µM) (Figure 2A). 100 µM PFOA treatment resulted in an increase in LDH release in the supernatants, which peaked at Day-9, however this increase did not reach statistical significance. After Day-9, LDH declined with 100 µM PFOA consistent with fewer numbers of viable cells as confirmed by microscopic evaluation. As such, overtly cytotoxic concentrations were excluded from any further analyses.

PFOS was the most cytotoxic of the chemicals tested in the magnitude of LDH leakage and the speed at which cell death occurred at the high concentrations. As shown in Figure 2C, the cytotoxic effect was rapid with 50 µM and 100 µM PFOS causing dramatic cell death as early as 24 hrs post-exposure. After this time, the RLU ratios declined as a result of fewer viable cells as cell death progressed. After Day-6 the LDH release for this concentration was no longer different from the control, due to the decrease in surviving cells. For the 50 µM PFOS treatment, cytotoxicity occurred more gradually with an initial 50-fold increase in cytotoxicity after 24hrs, and significant cytotoxicity between Day-6 and Day-9, but no effect after Day 9. The lower concentrations of PFOS did not show any significant cytotoxicity. Based on these results, the 50 µM and 100 µM concentrations were both excluded from the gene expression analysis. Finally, PFBS (Figure 2B) and PFDS (Figure 2D) did not induce any measurable cytotoxicity with any of the concentrations over the 14 days of culture.

Data quality overview and removal of transcriptomic outliers

The gene expression data are available in the NCBI's Gene Expression Omnibus (Bioproject number PRJNA604830). Initial quality assessment was done on water-only controls and reference standards included on every TempO-Seq plate. We first confirmed very little signal (< 0.3%) from samples with no cells/RNA. In addition, we confirmed that commercial human universal reference RNA (two per plate – 16 in total) showed very high Spearman correlation coefficients (> 0.94) across all plate comparisons indicating a high degree of technical reproducibility across the plates.

The median read depth for the study was two million reads with a minimum read depth of 400,000. The cytotoxicity information above was paired with the number of

reads recovered during the TempO-Seq experiments to identify overtly cytotoxic concentrations for removal from the transcriptomic data analysis. The conditions removed from subsequent analyses were: 100 µM PFOA on days 10 and 14, and 50 µM on Day-14; 50 and 100 µM PFOS exposure from all time points. Hierarchical clustering was done to identify any additional outliers. This analysis led to the removal of a total of 106 samples, such that the sample size of the experiment was either n=3 or n=4 across every condition in the experiment, with an average of 16 DMSO controls per plate.

Differentially Expressed Genes (DEGs) and Cluster Analysis

Table1 summarizes the numbers of DEGs (FDR adj p-value ≤ 0.05 and |FC| ≥ 1.5) for each PFAS. As anticipated, the number of DEGs generally showed a trend toward increasing response with concentration, and to a lesser extent, time of exposure. PFOS exposure induced the greatest number of DEGs; whereas, PFBS induced very few DEGs overall across time, even at the highest concentration (largest number of DEGs was 87 on Day 4 at 100 µM). Comparing all PFAS at 20 µM, the highest non-cytotoxic concentration in common across all of the chemicals, revealed that the rank order for which PFAS induced the most transcriptional changes was consistent across time in the following order: PFOS > PFDS > PFOA > PFBS. There were minimal transcriptional alterations at the lowest concentrations; however, there was some indication for the possibility of non-monotonic responses (e.g., 86 DEGs for PFOS at 0.1 µM on day 1; and 30 genes for PFDS at 0.1 µM on day 10, Table 1).

Analysis of the DEGs for each PFAS at their top non-cytotoxic concentration (PFBS 100 µM, PFDS 100 µM, PFOA 20 µM, and PFOS 20 µM) revealed no genes in common on Day-1 (Supplemental File 2 Panel A); however, Days 4, 10, and 14 all had multiple DEGs in common. Analysis of the DEGs at a uniform concentration of 20 µM (Supplemental File 2 Panel B) did not include PFBS on Days 1 and 4, as they did not meet the restrictions cut offs within IPA analysis ($p<0.05$ and FC$\pm$1.5) and could not be included as such. The 20 µM analysis (Panel B) revealed that on Days 1 and 4 had 8 and 33 genes (respectively) were in common over the 3 chemical treatments. Of

particular interest is Perilipin-2 (PLIN2), a lipid droplet associated protein involved in the storage of fats, appears in several of the lists as a commonly affected genes.

PCA was conducted at each time point to explore general relationships in the transcriptional profiles induced by the PFAS using the DEGs (Figure 3). Quite generally, PC1 (the main driver of variability) appears to be based on concentration of the PFAS, with higher concentrations to the right on the plot and all lower concentrations together on the left. The PCAs over time demonstrate the marginal impact of PFBS on the liver spheroid transcriptome (grouping in with the low concentrations and controls). In addition, higher concentrations of PFOS and PFDS were more frequently in close proximity to each other than they were to PFOA. Similarly, hierarchal cluster analysis of the DEGs (Supplemental File 3) revealed that at the earlier time points, the exposure groups clustered by concentration as opposed to chemical. High concentrations of PFOA, PFBS, PFOS, and PFDS were more likely to be on a branch together than samples within the same chemical exposure. This trend continued on day 4 and 10; however, by day 14 the PFAS were more likely to be clustered based on chemical and concentration.

Functional Analysis and upstream regulators

Pathway (i.e., gene sets) analyses were conducted in IPA using the DEGs from the 20 µM concentration (the top non-cytotoxic concentration in common across all the PFAS) (Figure 4A) or the top non-cytotoxic concentration (Figure 4B) across all chemicals and time points. This analysis revealed that most pathways affected by PFAS were downregulated based on IPA predictions that factor in the directionality of the expression changes. Overall, there was a remarkably similar pattern of pathway enrichment for PFOS and PFDS that was different from PFOA and PFBS.

PFOS and PFDS pathway analyses suggest that the exposures cause inhibition of LXL/RXR activity, as well as the mevalonate and cholesterol biosynthesis pathways, which all appear to persist across time. In contrast, PFOA treatment appears to strongly activate stearate biosynthesis and fatty acid beta oxidation pathways. Unlike the other PFAS, PFBS displayed such small proportions of gene expression changes that it did not perturb any canonical pathways up to 20 µM. However, the 100 µM concentration of

PFBS elicited a strong upregulation of several pathways at the 10 and 14-day time points (Figure 4B) including stearate biosynthesis, fatty acid oxidation, acetone degradation, estrogen biosynthesis, bupropion degradation, nicotine degradation, and the melatonin degradation pathway.

A detailed overview of perturbed pathways over all concentrations and time points for each PFAS is beyond the scope of this study, which is geared more toward analysis of general trends/patterns across the data. However, concentration-response for the pathway analysis is shown for PFOS as an illustration (Supplemental File 4). This analysis supported the general trend of increasing pathway perturbations at higher concentrations (with the exception of 0.1 µM on day 1), and consistency in response of specific pathways across concentration and time including inhibition of cholesterol biosynthesis, LXR/RXR activation, melatonin degradation and nicotine degradation pathways (Supplemental File 4).

Upstream regulators represent potential key mediators of the DEGs and provide additional insight into mode of action. We restricted this analysis to the upstream regulators with a z-score filter of $\pm$ absolute 3.0 and a Benjamini Hochberg adjusted p-value of 0.05 to focus on the most impacted regulators. Applying these stringent filters, peroxisome proliferator-activated receptor alpha (PPARα) was predicted to be an activated upstream regulator for all four PFAS over all time points (Figure 5). Indeed, PPARα was predicted by the IPA database to have increased activity in all PFAS exposures to varying degrees. Of the predicted inhibited upstream regulators, Copper-transporting ATPase 2 (ATP7B), sterol regulatory element-binding transcription factor 1 and 2 (SREB 1 and SREB 2), sterol regulatory element-binding protein cleavage-activating protein (SCAP), and Insulin Receptor (INSR) were all predicted to be inhibited at all-time points with PFOS and PFDS. Interestingly, these upstream regulators were also predicted to be inhibited (but more weakly) with PFOA at the four and ten-day time points. Overall, there was a strikingly consistent pattern of upstream regulator activation/inhibition between PFOS and PFDS that differed from the other two PFAS.

Benchmark Concentration Analysis

To compare potencies across the PFAS, we conducted a transcriptional BMC analysis with a BMR of one standard deviation. To broadly compare potencies, median BMCs for all genes that could be obtained from best-fit models within BMDExpress were derived along with a bootstrapped 95% confidence interval (Figure 6). PFOS consistently had a BMC between 6.3 to 7.3 µM across all time points, with narrow confidence intervals. There was some variability across time in the BMCs of the other PFAS. The BMCs of both PFOA and PFDS on Day-1 were significantly higher than PFOS (non-overlapping confidence intervals); however, by day 14 PFOS, PFOA, and PFDS were in the same range with overlapping confidence intervals, suggesting equal potencies. PFBS BMCs ranged from 43.2 to 73.9 µM (Supplemental File 5).

Gene accumulation plots show the BMCs for each of the genes that could be modeled (Figure 7). Note that overtly cytotoxic concentrations were not modeled, thus some curves terminate at lower concentrations than others (i.e., 20 µM for all PFOS time points, and 20 µM for PFOA for day 10 and 14). The plot demonstrates again that PFOS induces the most transcriptional changes at all time points (highest on y-axis and shifted furthest to the left on the x-axis), with BMCs at lower concentrations; whereas, PFBS induces the least transcriptional perturbations and at higher concentrations than the other three PFAS. Notably, transcriptional activity for PFOS, PFOA, and PFDS converge at the origin, indicating that biological changes in the 'most sensitive' genes are induced in a similar concentration range.

Bioactivity Exposure Ratio (BER)

The BER is the ratio of the administered equivalent dose (AED) for the NAM POD to population exposure for a given chemical. A large BER value is an indication of lower risk, whereas a lower value indicates increased risk to human health (Wetmore *et al.*, 2015b; Paul Friedman *et al.*, 2020). However, the use of transcriptomics in risk assessment is a relatively new concept and there is lack of consistency in how to derive the POD for a given chemical (e.g., selected genes, gene-sets, or pathways), wherein the approach used to determine the AED influences the scale of the BER estimate. Recognizing this lack of standardization, (Farmahin *et al.*, 2017) demonstrated that there is general consistency between most methods that allowed for reproducible

determinations of transcriptional PODs. This was taken into account by comparing two conservative approaches. For **Approach 1**, a POD that is comparable to previous approaches used for ToxCast data was applied: the 5th percentile gene BMC (Paul Friedman *et al.*, 2020). **Approach 2** was based on data demonstrating a strong correlation between the dose at which apical effects *in vivo* occur and the lowest (most sensitive) *in vivo* pathway BMC (Thomas *et al.*, 2013). Here, BERs were derived by dividing the AED for each transcriptomic POD approach to exposure taken from the US population (Figure 8). The BERs for each approach (approach 1, blue diamond; approach 2, red diamond) were then compared to a range of endpoints derived from animal exposure data used in risk assessment guidelines (green crossbar) at each time point for PFOA and PFOS (Table 2). As previously mentioned the other (PFBS and PFDS) were excluded from BER calculation due to limited exposure data available for US and Canadian populations.

For PFOA, AED values slightly increased from Day-1 to Day-4 and then decreased by day 14 for both BER approaches (Figure 8). The calculated BERs for approach 1 were within a 2-orders of magnitude margin of the population exposure with a range 121 to 442, except for a day 14 BER of 39 (Table 2). Although more conservative, the second approach generally decreased the BER by an order of magnitude with a range of 28 to 42 except for a Day-4 BER of 135 (Table 2). The reference BER for PFOA (105) was derived using the lowest endpoint in Health Canada's drinking water guidelines: BMD_{10} for induction of hepatocellular hypertrophy in rats (Health Canada, 2018a). This animal *in vivo* BER was within the same order of magnitude of approach 1 (Table 2).

For PFOS, AED values remained relatively constant for both approaches over all measured time points (Figure 8). The BERs in Table 2 for approach 1 (range of 53 to 151) was within 1 to 2 orders of magnitude and were similar to the more conservative approach 2 (range 82 to 115). The reference BER for PFOS (44) was derived using the lowest endpoint from Health Canada's drinking water guidelines: the NOAEL for induction of hepatocellular hypertrophy in rats (Health Canada, 2018b). This animal *in*

vivo data-derived BER was within range of both transcriptomic approaches and an order of magnitude lower than the PFOA BER (Table 2).

Discussion

This study shows the utility of the human liver spheroid model paired with transcriptional profiling as an alternative approach to toxicological assessment of PFAS. Four prototype PFAS representing short, medium and long-chain PFAS were examined using a detailed concentration-response analysis across four time points. The extent of transcriptional changes induced by PFOS was larger than any of the other PFAS, with transcriptional perturbations declining in the following order (based on DEGs at 20 µM): PFOS > PFDS > PFOA > PFBS. Interestingly the median transcriptomic BMCs of PFOS, PFDS, and PFOA were highly overlapping at the later time points. The lowest transcriptomic BMCs were highly similar across these three PFAS, suggesting fairly equal potencies. In addition, pathway and upstream regulator analysis clearly revealed that although all the PFAS expression profiles were consistent with activation of PPARα, PFOS and PFDS were more similar to each other. Indeed, PFOS and PFDS induced remarkably similar pathway alterations (described in more detail below). In contrast, the short-chain PFAS (PFBS) induced marginal changes in transcriptional activity and was much less potent than the C-8s and C-10 PFAS. These data serve as a critical baseline for comparison of data-poor PFAS and for developing read-across approaches in this human liver cell model.

Functional analysis of the DEGs suggests that PPARα plays a role in mediating the toxic effects of PFAS in human liver spheroids. PPARα was predicted to be an upstream regulator from which other genes are transcriptionally activated across all the PFAS and time points. PPARs are nuclear receptors involved in regulation of energy homeostasis and expression of numerous genes involved in lipid metabolism (Janssen *et al.*, 2015; Liss and Finck, 2017). In humans, PPARα is a regulator of lipogenesis and glucose metabolism in the liver (Janssen *et al.*, 2015) Dose-dependent up-regulation of PPARα expression with increasing PFOS exposure has been observed in rodents (Ye *et al.*, 2012). Likewise, increased PPARα activity in rodents has been associated with exposure to PFOA and PFOS (Rosen *et al.*, 2008, 2010). However, the same studies found that PPARα knock-out mice also had altered lipid metabolism pathways,

indicating that there are PPARα-independent mechanisms through which PFAS operate (Rosen *et al.*, 2008, 2010; Abbott *et al.*, 2009). Our data support that PPARα activity is increased in response to PFAS exposure in human liver spheroids, but that there are other upstream regulators that are likewise affected.

PFOA, PFOS, and PFDS all appear to inhibit several upstream regulators. Inhibition of ATP7B, an ATPase copper protein transporter required for the transport of copper to the bile, is predictive of copper accumulation in hepatocytes, which can lead to liver toxicity (Bartee and Lutsenko, 2007). Inhibition of sterol regulatory binding factors 1 and 2 (SREP 1 and 2), and sterol regulatory element-binding protein cleavage – activating protein (SCAP), both of which are part of the cholesterol, fatty acids, and triglycerides synthesis pathways (Moslehi and Hamidi-zad, 2018), suggest a downregulation of lipogenesis. Perturbation of these pathways is potentially adaptive; i.e., as PPARα is activated, SREBP1,2 and SCAP are downregulated in an attempt to reach homeostasis of lipid accumulation. Finally, suppression of the insulin receptor (INSR), an activator of the SREBP 1 transcription factor, suggests that PFAS exposure affects the insulin signalling pathway and thus inhibits normal lipogenesis further. Over time, disruption of cholesterol efflux into the intestine can cause cholestasis, liver inflammation, steatosis, and ultimately liver disease (Vrins *et al.*, 2012; Utzschneider and Kahn, 2006).

Interestingly, despite some similarities, PFOA had a broadly different pattern of transcriptional pathway alterations. PFOS and PFDS exerted major effects on the transcription of genes involved in cholesterol biosynthesis. In contrast, PFOA appeared to upregulate the stearate biosynthesis I pathway, in parallel with the fatty acid-ß oxidation pathway. Similarly, Das et al. (2017) found that exposure of wild type and PPARα-null mice to PFOA (among other PFAS) resulted in increased fatty acid accumulation/synthesis favoring fat accumulation in the liver. Upregulation of the fatty acid-ß oxidation pathway after PFOA exposure has also been reported in Balb/c mice (Yu *et al.*, 2016) and in Wistar rats (Haughom and Spydevold, 1992). Although upregulation of the stearate biosynthesis pathway, at the same time as upregulation of the oxidation or breakdown of fatty acids, seems counterproductive, we speculate that PFOA is causing dysregulation of pathways involved in lipid homeostasis in the liver.

The seemly duality of this response may be an attempt to counterbalance lipid accumulation in the liver and to react to the effects of the exposure. Overall, although fairly equal in potency, PFOA appears to operate through different mechanisms to PFOS and PFDS, suggesting that it may be advisable to consider this carboxylate separately from the longer-chain PFAS with sulfonic acid functional groups for the purposes of risk assessment.

PFBS exposure is clearly less potent and biologically active, with its lowest BMC an order of magnitude greater than the other PFAS. Indeed, PFBS only activated pathways at the highest concentrations and later time points. Naile et al. (2011) studying the effects of 10 PFAS commonly found in the environment on rat hepatocyte cells, found that genes involved in fatty acid synthesis, cholesterol synthesis, and thyroid development are uniquely affected by the different PFAS (Naile *et al.*, 2012). Importantly, chain length impacted transcriptomic profiles, with shorter chain length PFAS having less transcriptional perturbations. This study as well as others support our finding that PFBS has a different and weaker transcriptomic response.

The above transcriptomic findings are highly consistent with demonstrated effects of PFAS on cholesterol, lipid synthesis and metabolism in various other model organisms. Although data for most PFAS are limited, exposure in rodents to PFOS and PFOA clearly illustrate changes in fatty acid production, cholesterol synthesis, and lipid homeostasis leading to cholestasis/steatosis (Das *et al.*, 2017; L. Wang *et al.*, 2014; Bijland *et al.*, 2011; Du *et al.*, 2009; Peden-Adams *et al.*, 2009; Wan *et al.*, 2012)(Curran *et al.*, 2008; Louisse *et al.*, 2020). In keeping with these effects, obese participants from the National Health and Nutrition Examination Survey (2011-2014) exhibit a positive association of PFOA, PFHxS and PFNA with major liver biomarkers associated with steatosis (Jain and Ducatman, 2019). These findings support the relevance of our results for exposed humans. Overall, our short-term *in vitro* transcriptomic study point to the same genes/pathways/disease outcomes as predicted by *in vivo* studies and associated human data.

BMC analysis was conducted to compare potencies of the four PFAS. Although PFOS initially appeared to be the most potent for median gene BMCs, by day 14, PFDS

and PFOA were equipotent with PFOS. Permeability and uptake of PFOS has been found to be much faster than PFBS in human lung epithelial and murine preadipocyte embryonic fibroblasts (Sanchez Garcia *et al.*, 2018). Furthermore, both active and passive transport mechanisms for PFOA have been identified in isolated rat hepatocytes (Han *et al.*, 2008) and in the human colorectal adenocarcinoma cell line Caco-2 (Kimura *et al.*, 2017). Based on the premise of selective uptake and concentration of different PFAS, it is reasonable to speculate that differences in PFAS potencies over time may be influenced in part by the kinetics of cellular uptake and permeability. One limitation of this study was that we were not able to measure the concentration of PFAS within the spheroids. Future studies will examine internal concentrations of PFAS within the spheroids over time. Overall, these baseline data can be used for rank potency comparisons with other PFAS.

Another way of exploring the potency is by focusing on the lowest gene BMCs. Using this approach, we see convergence at the far-left side of the accumulation plots, indicating more consistency in the BMCs between the chemicals over time. Thus, looking at the lowest gene or pathway BMC may reduce the need to conduct experiments across a large time span, which would be useful if high-throughput screening is the intention.

Pharmacokinetic and exposure information were only available for PFOS and PFOA to derive BERs. The two approaches used (Approach 1: 5th percentile gene BMC and Approach 2: lowest pathway median gene BMC) yielded results that were highly consistent with the apical endpoint BER, lending confidence to these approaches. There were also commonalities in the lowest median pathway BMCs across the PFAS: fatty acid activation and ubiquinol-10 biosynthesis. These pathways are also consistent with the literature indicating that both PFOS (Reif *et al.*, 2010) and PFOA (Das *et al.*, 2017) leads to hepatic steatosis (i.e., fatty liver disease), providing confidence in this selected POD. Steatosis was highlighted as an important endpoint within the US EPA's Integrated Risk Information System (IRIS) on PFOS/PFOA and is recognized as a key step in the liver disease progression (Kaiser *et al.*, 2012). Wetmore et al. proposed that a BER cut-off < 100 suggests that the AED of biological activity is significantly different from daily population exposure estimates (Wetmore *et al.*, 2015b). Our study yielded

BERs that are <100, indicating that there is a relatively narrow margin between highly exposed members of the US population and activity *in vitro* for PFOS and PFOA.

International government agencies are striving to implement recommendations made in the seminal document Toxicology Testing for the 21 Century (Krewski 2019). This study developed a transcriptomic pipeline to distinguish similarities and differences between PFAS that can be used to inform hazard, mode of action, and potency. The data and approach are now being used at Health Canada to assess additional data-poor PFAS (manuscript in preparation). High-throughput transcriptomics is of considerable value because it broadly informs global biological perturbations induced by chemical exposures.

Acknowledgements

We thank Dr. Francesco Marchetti, Dr. Marc Beal and Dr. Scott Auerbach for their helpful commentary and review of this research, the US EPA for their valuable consultations, as well as BioSyder for their contributions on this project.

Funding

We acknowledge the Water and Air Quality Bureau, HECSB, Health Canada, the Chemicals and Environmental Health Management Bureau, HECSB, Health Canada, and Environmental Health Sciences & Research Bureau, HECSB, Health Canada who jointly funded this research.

TABLES

Table 1. Differentially Expressed Genes (DEGs) in the PFAS-treated spheroids relative to control over each time point and concentration.

PFAS	DAY	0.02uM	0.1uM	0.2uM	1uM	2uM	10uM	20uM	50uM	100uM
PFOA	1	0	8	36	8	19	81	72	236	490
	4	1	0	17	26	12	32	73	196	873
	10	15	7	2	4	11	85	106	625	CYTOTOXIC
	14	2	1	3	2	9	68	94	CYTOTOXIC	CYTOTOXIC
PFBS	1	0	1	0	5	6	49	0	44	74
	4	7	2	0	15	0	3	0	23	87
	10	2	1	0	1	2	0	7	55	79
	14	0	0	0	0	0	4	1	2	75
PFOS	1	1	86	3	6	51	174	299	CYTOTOXIC	CYTOTOXIC
	4	0	3	8	20	37	260	305	CYTOTOXIC	CYTOTOXIC
	10	1	86	3	6	51	174	299	CYTOTOXIC	CYTOTOXIC
	14	0	0	8	8	9	265	398	CYTOTOXIC	CYTOTOXIC
PFDS	1	0	1	0	6	22	61	83	182	190
	4	0	3	0	2	5	276	225	230	284
	10	0	30	0	45	42	140	181	241	237
	14	1	2	1	5	102	184	186	198	391

Table 2. AEDs and BERs derived from Approaches 1 and 2 and reference values from animal models using Health Canada drinking water guidelines for PFOA and PFOS.

			Reference Values		**Approach 1**		**Approach 2**		
			(Animal) Health Canada guidelines		Lowest 5th percentile		Median AED of the gene-set from the most sensitive pathway		
	Day	Population Exposure (mg/kgBW/day)	AED (mg/kgBW/day)	BER	AED (mg/kgBW/day)	BER	AED (mg/kgBW/day)	BER	Pathway
PFOS	01	4.76e-04	0.021	44	0.043	90	0.042	88	Glutathione mediated detoxification
	04	4.76e-04	0.021	44	0.026	53	0.052	108	Ethanol degradation II
	10	4.76e-04	0.021	44	0.049	102	0.055	115	Antigen presentation pat
	14	4.76e-04	0.021	44	0.072	151	0.039	82	Fatty acid activation
PFOA	01	4.50e-04	0.050	105	0.084	187	0.013	28	Ubiquinol-10 biosynthes (eukaryotic)
	04	4.50e-04	0.050	105	0.199	442	0.061	135	Fatty acid activation
	10	4.50e-04	0.050	105	0.054	121	0.019	42	Ubiquinol-10 biosynthes (eukaryotic)
	14	4.50e-04	0.050	105	0.018	39	0.013	30	Stearate biosynthesis I (animals)

Animal BER = (Animal AED / Population exposure level)

Approach 1 BER = (Lowest 5th percentile gene AED / Population exposure level)

Approach 2 BER = (Median gene-level BMD of lowest pathway AED / Population exposure level)

REFERENCES

Abbott, B.D. *et al.* (2009) Developmental toxicity of perfluorooctane sulfonate (PFOS) is not dependent on expression of peroxisome proliferator activated receptor-alpha (PPARα) in the mouse. *Reproductive Toxicology*, **27**, 258–265.

Armitage, J. *et al.* (2006) Modeling global-scale fate and transport of perfluorooctanoate emitted from direct sources. *Environmental Science and Technology*, **40**, 6969–6975.

Armitage, J.M. *et al.* (2009a) Comparative assessment of the global fate and transport pathways of long-chain perfluorocarboxylic acids (PFCAs) and perfluorocarboxylates (PFCs) emitted from direct sources. *Environmental Science and Technology*, **43**, 5830–5836.

Armitage, J.M. *et al.* (2009b) Modeling the global fate and transport of perfluorooctanoic acid (PFOA) and perfluorooctanoate (PFO) Emitted from direct sources using a multispecies mass balance model. *Environmental Science and Technology*, **43**, 1134–1140.

Bach, C.C. *et al.* (2016) Perfluoroalkyl and polyfluoroalkyl substances and measures of human fertility: a systematic review. *Critical Reviews in Toxicology*, **46**, 735–755.

Bartee, M.Y. and Lutsenko, S. (2007) Hepatic copper-transporting ATPase ATP7B: Function and inactivation at the molecular and cellular level. In, *BioMetals*., pp. 627–637.

Biegel, L.B. *et al.* (2001) Mechanisms of Extrahepatic Tumor Induction by Peroxisome Proliferators in Male CD Rats.

Bijland, S. *et al.* (2011) Perfluoroalkyl sulfonates cause alkyl chain length-dependent hepatic steatosis and hypolipidemia mainly by impairing lipoprotein production in APOE*3-leiden CETP mice. *Toxicological Sciences*, **123**, 290–303.

Butenhoff, J.L. *et al.* (2012) Chronic dietary toxicity and carcinogenicity study with ammonium perfluorooctanoate in Sprague-Dawley rats. *Toxicology*, **298**, 1–13.

Canada. Health Canada. (2017) Water talk□: drinking water screening values□: perfluoroalkylated substances. Health Canada.

Chang, E.T. *et al.* (2014) A critical review of perfluorooctanoate and perfluorooctanesulfonate exposure and cancer risk in humans. *Critical Reviews in Toxicology*, **44**, 1–81.

Curran, I. *et al.* (2008) Altered fatty acid homeostasis and related toxicologic sequelae in rats exposed to dietary potassium perfluorooctanesulfonate (PFOS). *Journal of Toxicology and Environmental Health - Part A: Current Issues*, **71**, 1526–1541.

Das, K.P. *et al.* (2017) Perfluoroalkyl acids-induced liver steatosis: Effects on genes controlling lipid homeostasis. *Toxicology*, **378**, 37–52.

Du, Y. *et al.* (2009) Chronic effects of water-borne PFOS exposure on growth, survival and hepatotoxicity in zebrafish: A partial life-cycle test. *Chemosphere*, **74**, 723–729.

Eriksen, K.T. *et al.* (2013) Association between Plasma PFOA and PFOS Levels and Total Cholesterol in a Middle-Aged Danish Population. *PLoS ONE*, **8**.

Farmahin, R. *et al.* (2017) Recommended approaches in the application of toxicogenomics to derive points of departure for chemical risk assessment. *Archives of Toxicology*, **91**, 2045–2065.

Filgo, A.J. *et al.* (2015) Perfluorooctanoic Acid (PFOA)–induced Liver Lesions in Two Strains of Mice Following Developmental Exposures:PPARα Is Not Required. *Toxicologic Pathology*, **43**, 558–568.

Geiger, S.D. *et al.* (2014) The association between PFOA, PFOS and serum lipid levels in adolescents. *Chemosphere*, **98**, 78–83.

Guidelines for Canadian Drinking Water Quality Guideline Technical Document Perfluorooctanoic Acid (PFOA).

Han, X. *et al.* (2008) Uptake of perfluorooctanoate in freshly isolated hepatocytes from male and female rats. *Toxicology Letters*, **181**, 81–86.

Haughom, B. and Spydevold, O. (1992) The mechanism underlying the hypolipemic effect of perfluorooctanoic acid (PFOA), perfluorooctane sulphonic acid (PFOSA) and ciofibric acid.

Health Canada (2018a) Guidelines for Canadian Drinking Water Quality Guideline Technical Document Perfluorooctanoic Acid (PFOA).

Health Canada (2018b) Guidelines for Canadian Drinking Water Quality: Guideline Technical Document – Perfluorooctane Sulfonate (PFOS).

Ingenuity Pathway Analysis:https://www.youtube.com/watch?v=ub7GLpD8dPQ (2017) Quick Start Guide to Running Ingenuity Pathway Analysis (IPA).

Jain, R.B. and Ducatman, A. (2019) Selective Associations of Recent Low Concentrations of Perfluoroalkyl Substances with Liver Function

Biomarkers: NHANES 2011 to 2014 Data on US Adults Aged ≥20 Years. *Journal of Occupational and Environmental Medicine*, **61**, 293–302.

Janssen, A.W.F. *et al.* (2015) The impact of PPARαα activation on whole genome gene expression in human precision cut liver slices. *BMC Genomics*, **16**.

Joakim Ek, C. *et al.* (2015) Transcriptomal changes and functional annotation of the developing nonhuman primate choroid plexus. *Frontiers in Neuroscience*, **9**.

Kaiser, J.P. *et al.* (2012) Putative mechanisms of environmental chemical-induced steatosis. *International Journal of Toxicology*, **31**, 551–563.

Kavlock, R.J. *et al.* (2018) Accelerating the Pace of Chemical Risk Assessment. *Chemical Research in Toxicology*, **31**, 287–290.

Kielsen, K. *et al.* (2016) Antibody response to booster vaccination with tetanus and diphtheria in adults exposed to perfluorinated alkylates. *Journal of Immunotoxicology*, **13**, 270–273.

Kimura, O. *et al.* (2017) Uptake of perfluorooctanoic acid by Caco-2 cells: Involvement of organic anion transporting polypeptides. *Toxicology Letters*, **277**, 18–23.

Krewski, D. *et al.* (2020) Toxicity testing in the 21st century: progress in the past decade and future perspectives. *Archives of Toxicology*, **94**.

Linda S. Birnbaum (2018) DEPARTMENT OF HEALTH AND HUMAN SERVICES NATIONAL INSTITUTES OF HEALTH NATIONAL INSTITUTE OF ENVIRONMENTAL HEALTH SCIENCES Hearing on “The Federal Role in the Toxic PFAS Chemical Crisis.” *Hearing on “The Federal Role in the Toxic PFAS Chemical Crisis” Testimony before the Senate Committee on Homeland Security and Governmental Affairs*.

Liss, K.H.H. and Finck, B.N. (2017) PPARs and nonalcoholic fatty liver disease. *Biochimie*, **136**, 65–74.

Liu, Z. *et al.* (2017) Pollution pathways and release estimation of perfluorooctane sulfonate (PFOS) and perfluorooctanoic acid (PFOA) in central and eastern China. *Science of the Total Environment*, **580**, 1247–1256.

Louisse, J. *et al.* (2020) Perfluorooctanoic acid (PFOA), perfluorooctane sulfonic acid (PFOS), and perfluorononanoic acid (PFNA) increase triglyceride levels and decrease cholesterogenic gene expression in human HepaRG liver cells. *Archives of Toxicology*, **94**, 3137–3155.

Moslehi, A. and Hamidi-zad, Z. (2018) Role of SREBPs in Liver Diseases: A Mini-review. *Journal of Clinical and Translational Hepatology*, **6**, 1–7.

National Toxicology Program NTP NTP Monograph Immunotoxicity Associated with Exposure to Perfluorooctanoic Acid or Perfluorooctane Sulfonate (2016).

Paul Friedman, K. *et al.* (2020) Utility of in Vitro Bioactivity as a Lower Bound Estimate of in Vivo Adverse Effect Levels and in Risk-Based Prioritization. *Toxicological Sciences*, **173**, 202–225.

Paul, S. and Auer, C. (2000) 3M General Offices 3M Center.

Peden-Adams, M.M. *et al.* (2009) Developmental toxicity in white leghorn chickens following in ovo exposure to perfluorooctane sulfonate (PFOS). *Reproductive Toxicology*, **27**, 307–318.

Reif, D.M. *et al.* (2010) Endocrine profling and prioritization of environmental chemicals using toxcast data. *Environmental Health Perspectives*, **118**, 1714–1720.

Rosen, M.B. *et al.* (2010) Gene expression profiling in wild-type and PPARα-null mice exposed to perfluorooctane sulfonate reveals PPARα-independent effects. *PPAR Research*.

Rosen, M.B. *et al.* (2008) Gene Profiling in the Livers of Wild-type and PPARα-Null Mice Exposed to Perfluorooctanoic Acid. *Toxicologic Pathology*, **36**, 592–607.

Sanchez Garcia, D. *et al.* (2018) Cellular accumulation and lipid binding of perfluorinated alkylated substances (PFASs) – A comparison with lysosomotropic drugs. *Chemico-Biological Interactions*, **281**, 1–10.

Schenker, U. *et al.* (2008) Contribution of volatile precursor substances to the flux of perfluorooctanoate to the arctic. *Environmental Science and Technology*, **42**, 3710–3716.

Shi, Y. *et al.* (2015) Characterizing direct emissions of perfluoroalkyl substances from ongoing fluoropolymer production sources: A spatial trend study of Xiaoqing River, China. *Environmental Pollution*, **206**, 104–112.

Stemmler, I. and Lammel, G. (2010) Pathways of PFOA to the Arctic: Variabilities and contributions of oceanic currents and atmospheric transport and chemistry sources. *Atmospheric Chemistry and Physics*, **10**, 9965–9980.

Thomas, R.R. *et al.* (2013) Temporal concordance between apical and transcriptional points of departure for chemical risk assessment. *Toxicological Sciences*, **134**, 180–194.

Trejo, C.L. *et al.* (2019) Extraction-free whole transcriptome gene expression analysis of FFPE sections and histology-directed subareas of tissue. *PLoS ONE*, **14**.

United States Environmental Protection Agency (2020) US EPA action plan on PFAS: program update. *https://www.epa.gov/pfas/pfas-action-plan-program-update-february-2020*.

Utzschneider, K.M. and Kahn, S.E. (2006) Review: The role of insulin resistance in nonalcoholic fatty liver disease. *Journal of Clinical Endocrinology and Metabolism*, **91**, 4753–4761.

Vrins, C.L.J. *et al.* (2012) Trans-intestinal cholesterol efflux is not mediated through high density lipoprotein. *Journal of Lipid Research*, **53**, 2017–2023.

Wambaugh, J.F. *et al.* (2013) Dosimetric anchoring of In vivo and In vitro studies for perfluorooctanoate and perfluorooctanesulfonate. *Toxicological Sciences*, **136**, 308–327.

Wan, H.T. *et al.* (2012) PFOS-induced hepatic steatosis, the mechanistic actions on β-oxidation and lipid transport. *Biochimica et Biophysica Acta - General Subjects*, **1820**, 1092–1101.

Wang, L. *et al.* (2014) PFOS induced lipid metabolism disturbances in BALB/c mice through inhibition of low density lipoproteins excretion. *Scientific Reports*, **4**.

Wang, T. *et al.* (2016) Levels, Isomer Profiles, and Estimated Riverine Mass Discharges of Perfluoroalkyl Acids and Fluorinated Alternatives at the Mouths of Chinese Rivers. *Environmental Science and Technology*, **50**, 11584–11592.

Wang, Z. *et al.* (2014) Global emission inventories for C4-C14 perfluoroalkyl carboxylic acid (PFCA) homologues from 1951 to 2030, Part I: Production and emissions from quantifiable sources. *Environment International*, **70**, 62–75.

Wania, F. (2007) A global mass balance analysis of the source of perfluorocarboxylic acids in the Arctic Ocean. *Environmental Science and Technology*, **41**, 4529–4535.

Wetmore, B.A. *et al.* (2015a) Incorporating high-throughput exposure predictions with dosimetry-adjusted in vitro bioactivity to inform chemical toxicity testing. *Toxicological Sciences*, **148**, 121–136.

Wetmore, B.A. *et al.* (2015b) Incorporating high-throughput exposure predictions with dosimetry-adjusted in vitro bioactivity to inform chemical toxicity testing. *Toxicological Sciences*, **148**, 121–136.

Ye, L. *et al.* (2012) Gene expression profiling in fetal rat lung during gestational perfluorooctane sulfonate exposure. *Toxicology Letters*, **209**, 270–276.

Yu, N. *et al.* (2016) Effects of Perfluorooctanoic Acid on Metabolic Profiles in Brain and Liver of Mouse Revealed by a High-throughput Targeted Metabolomics Approach. *Scientific Reports*, **6**.

Zanger, U.M. and Schwab, M. (2013) Cytochrome P450 enzymes in drug metabolism: Regulation of gene expression, enzyme activities, and impact of genetic variation. *Pharmacology and Therapeutics*, **138**, 103–141.

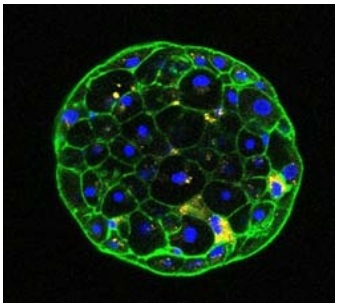

Figure 1A. Liver spheroids morphology after 4 days of treatment with 0.1% DMSO. Immunofluorescence staining with CD-68 for Kupffer cells (yellow), with phalloidin for F-actin filaments (green), and DAPI for nuclei (blue). 400x magnification.

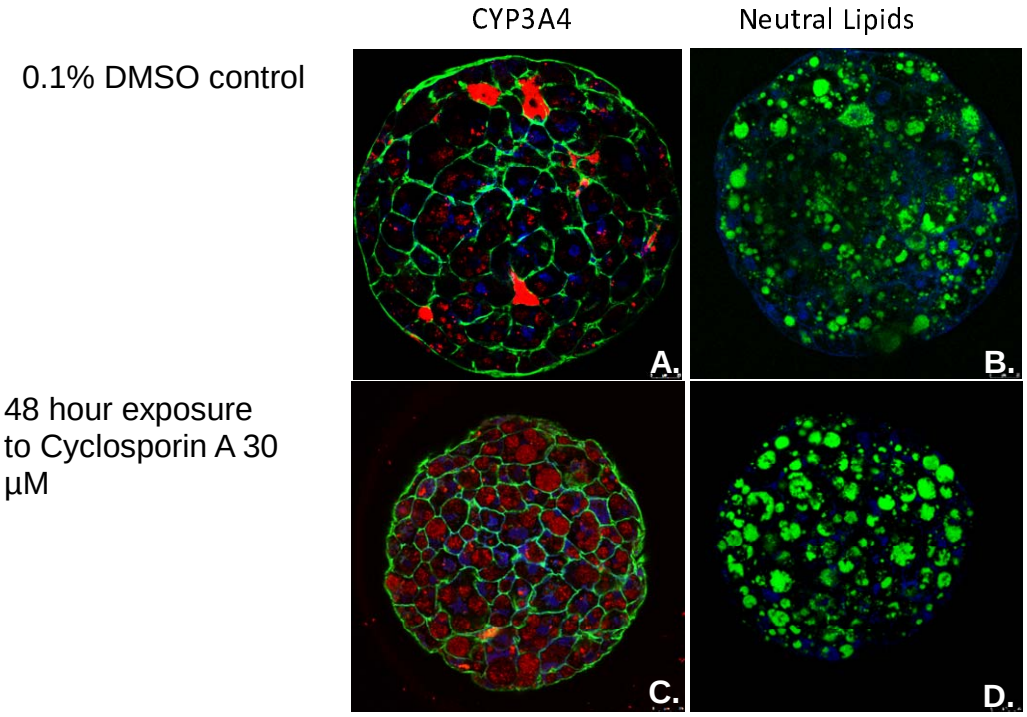

Figure 1B. Effects of 48-hour exposure to Cyclosporine A on spheroid morphology compared to DMSO control. Microscopy images are reflective of expected detoxification and increased activity of the detoxification/biotransformation of the spheroids. (A and C) Immunofluorescence staining for: CYP3A4–(red), F-actin filaments stained with phalloidin (green), and nuclei with DAPI(blue). (B and D) Immunofluorescence staining for: neutral lipids (green), and nuclei with DAPI (blue). 400x magnification.

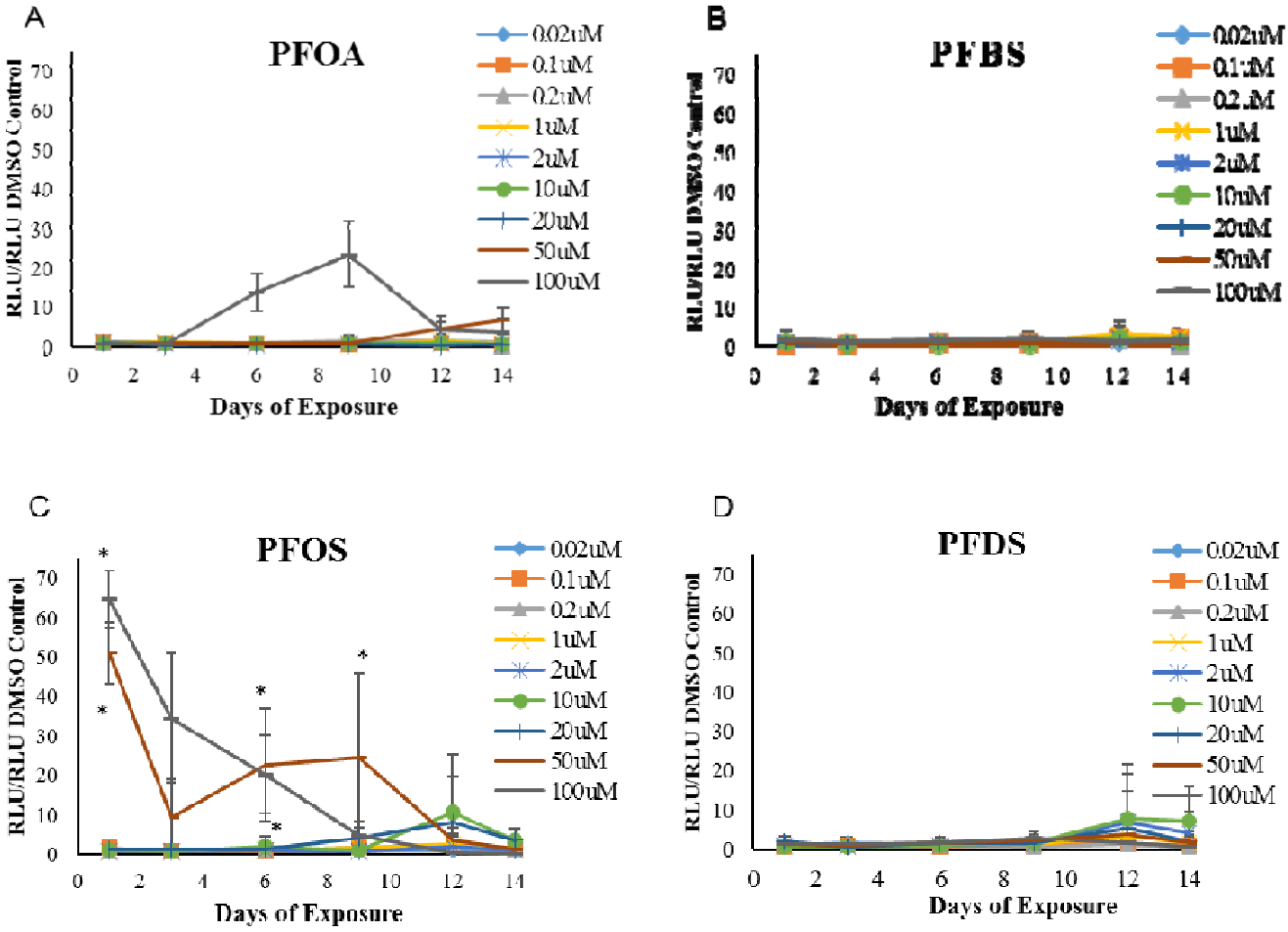

Figure 2. Lactate dehydrogenase (LDH) release as an indicator of cytotoxicity following treatment with a) PFOA b) PFBS c) PFOS or d) PFDS over a 14-day time course. Plots demonstrate the means +/- standard deviation of the ratio of sample RLU to mean DMSO RLU. * indicates the RLU was significantly higher than the DMSO control group ($p < 0.05$). Note that after reaching a peak, LDH levels decline over time consistent with reduced numbers of viable cells or evolving tolerance to chemical exposures in the spheroids.

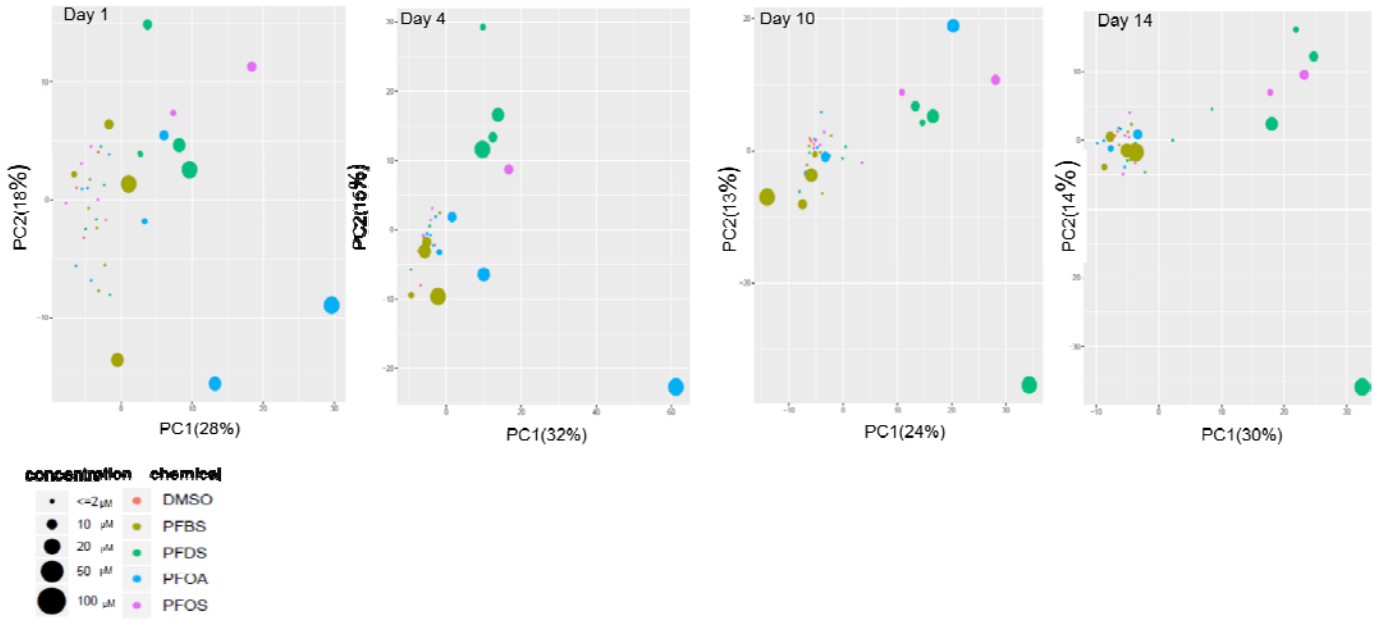

Figure 3. Principal Component Analysis (PCA) at each of the 4 time points. Size of dot represents the increasing concentrations; colours represent the four different PFAS.

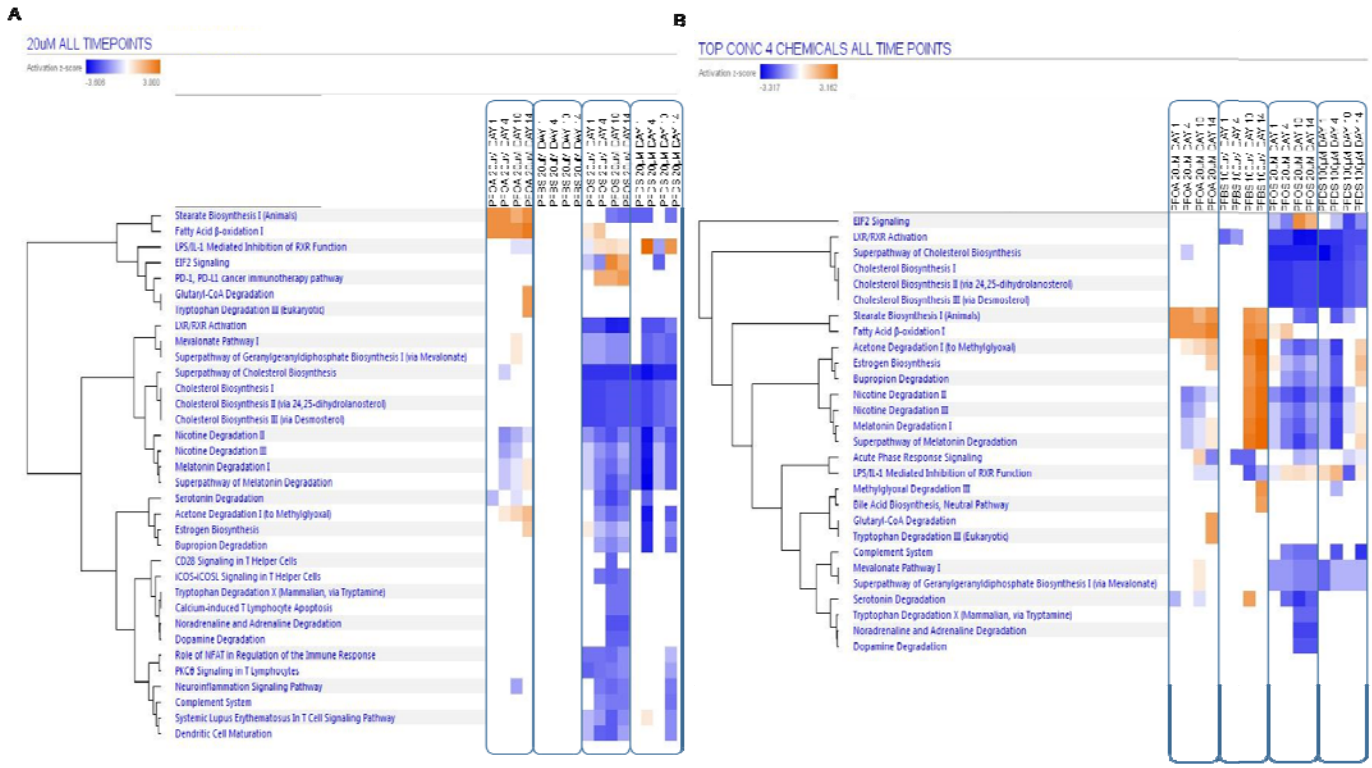

Figure 4. Pathway analysis of the DEGs for all time points at the 20 µM concentration (A) or for the highest non-cytotoxic concentration (B). Concentrations in (B) were 20 µM for PFOA and PFOS, and 100 µM for PFBS and PFDS. Filters for this analysis were set to z-score ≥ absolute 2.0 and Benjamini–Hochberg adjusted p-value ≤ 0.05. Blue represents inhibited pathways and orange represents activated pathways.

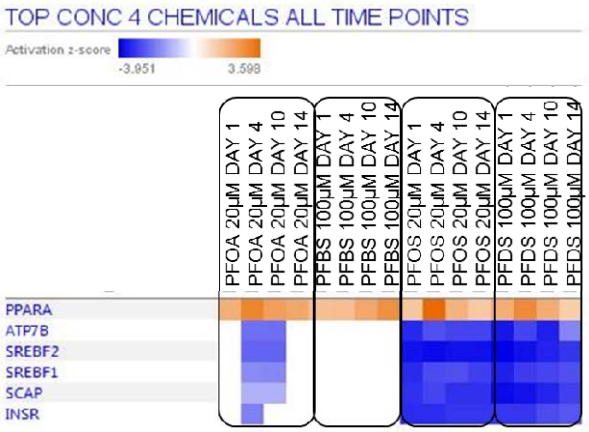

Figure 5. Upstream regulator predictions from the DEGs for the top non-cytotoxic concentration of each PFAS. The z-score filters were set to 3.0 with a Benjamini Hochberg adj p-value of 0.05 for this analysis. Blue represents inhibited upstream regulators, and orange represents activated regulators.

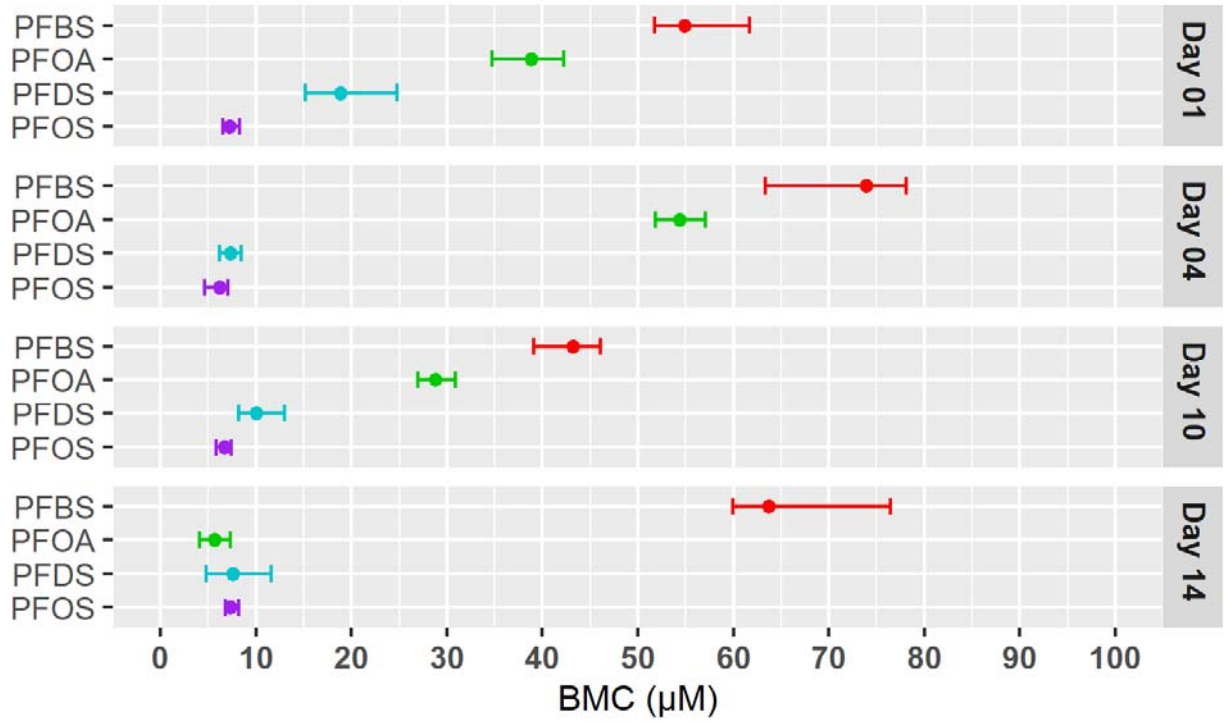

Figure 6. Median overall gene BMC (coloured dot) for all the genes that could be modeled and 95% confidence intervals for each of the PFAS.

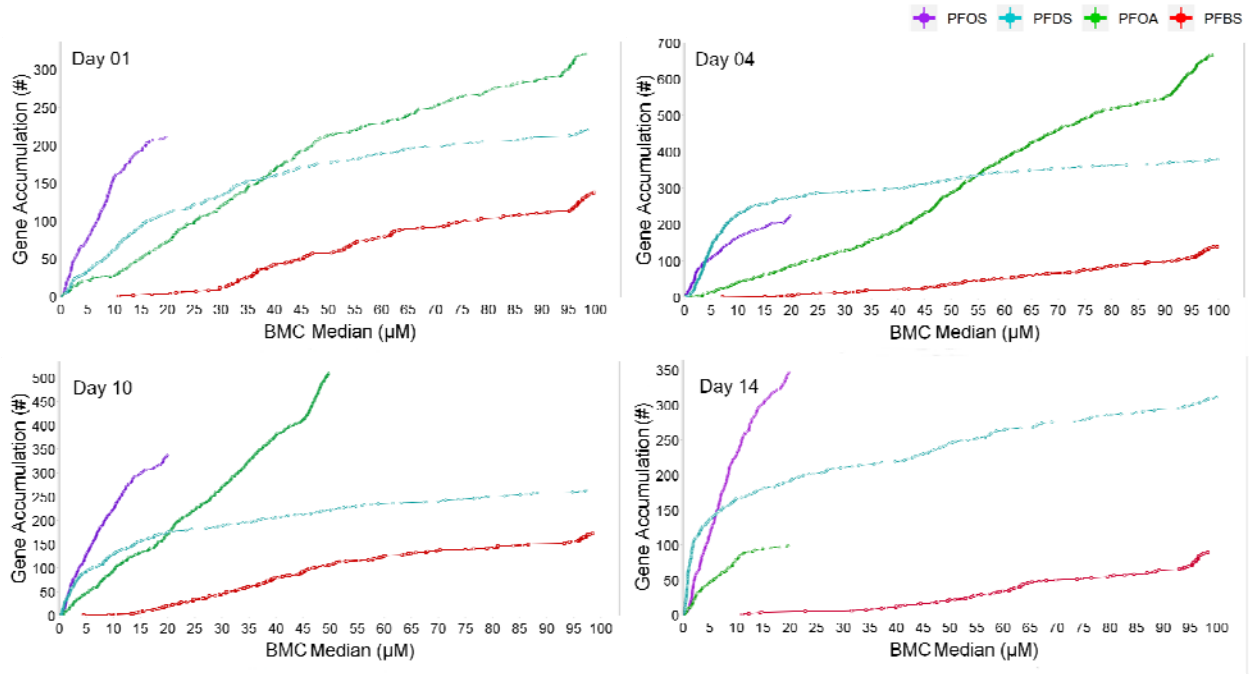

Figure 7. Gene accumulation plots showing the BMCs for each gene that could be modeled for each of the PFAS across time points.

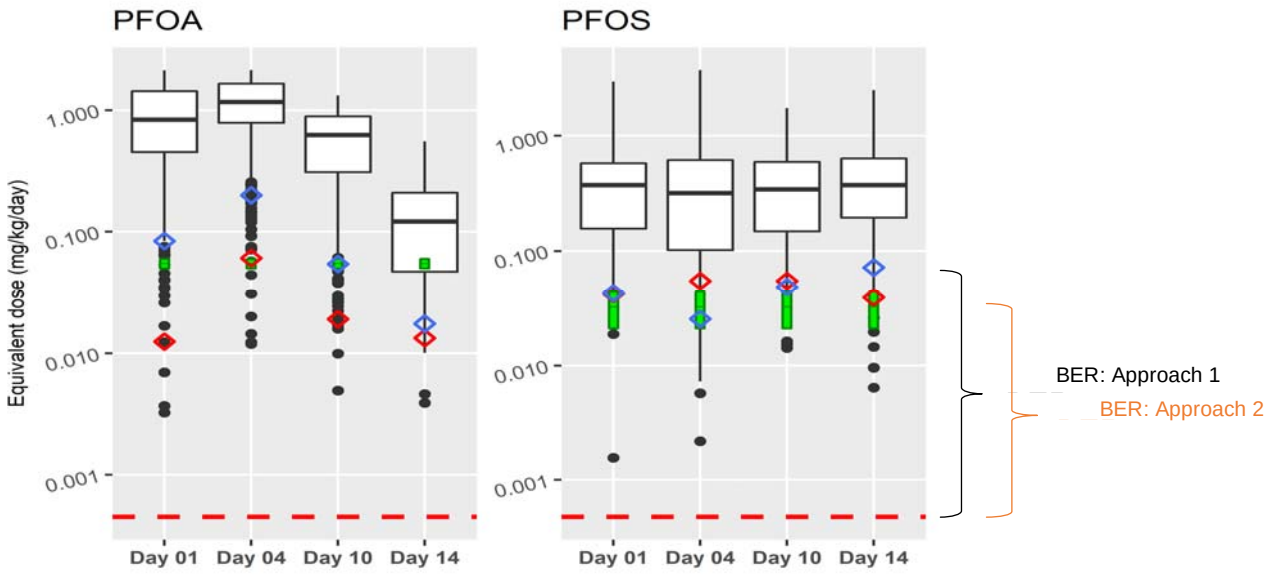

Figure 8. Boxplot of AEDs (mg/kg-BW/day) for PFOA and PFOS used to determination of BER from either the lowest 5th percentile BMC (blue diamond) or the median AED of the gene-set from the most sensitive pathway (red diamond) and compared with the estimated daily exposure of the upper limit of the daily US population exposure (95th percentile) obtained from the US EPA comptox dashboard (red dash). An AED derived from animal *in vivo* point of departure data (green crossbar) from Health Canada drinking water guidelines was included for reference.

SUPPLEMENTAL FILES

For DMSO 0.3%
newProbeLog2CPMvalue = log2(probeCPMvalue) - [log2(mean(DMSO0.3)) – log2(mean (DMSO0.1)]
For DMSO 0.17%
newProbeLog2CPMvalue = log2(probeCPMvalue) - [log2(mean(DMSO0.17)) – log2(mean (DMSO0.1)]
If a plate correction was made:
Data were 2^x, then
newProbeLog2CPMvalue = log2(probeCPMvalue) - [log2(mean(DMSO0.1ForPlateX)) – log2(mean(DMSO0.1ForAllPlates))]
in order to correct for the plate effect.

Supplemental File 1. Pipeline code

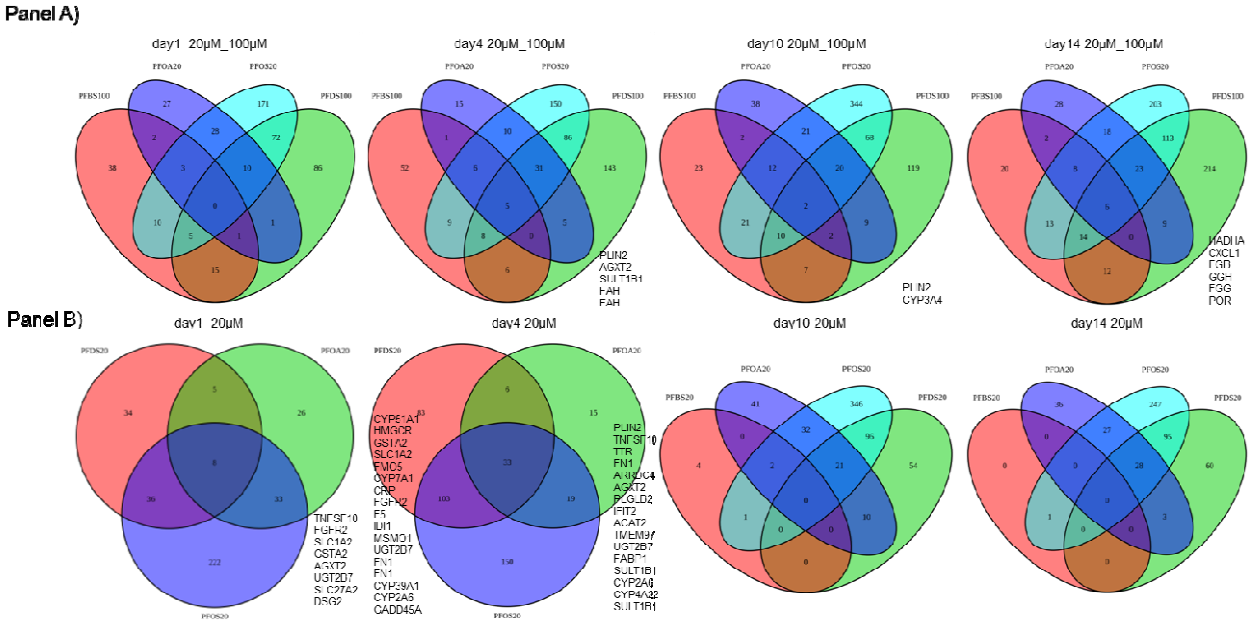

Supplemental File 2. Venn diagrams of DEGs illustrating gene lists that were found to be in common over treatments and time. Panel A) Analysis of the DEGs for each PFAS at their top non-cytotoxic concentration (PFBS 100 µM, PFDS 100 µM, PFOA 20 µM, and PFOS 20 µM). Panel B) Analysis of the DEGs for each PFAS at the 20 µM concentration. On Days 1 and 4 of the DEG lists for PFBS were not included, as they did not meet the restrictions cut offs within IPA analysis ($p<0.05$ and FC+1.5).

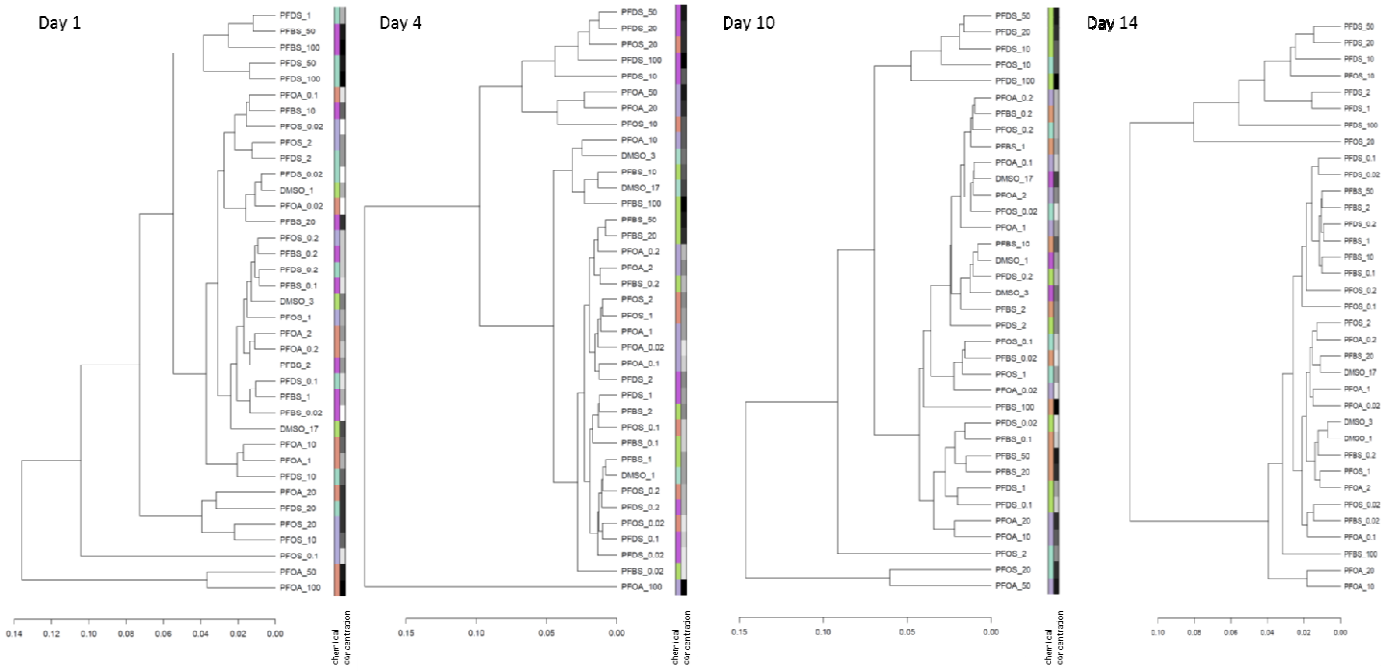

Supplemental File 3. Hierarchical clustering of differentially expressed genes from the four PFAS for all concentrations at each time point.

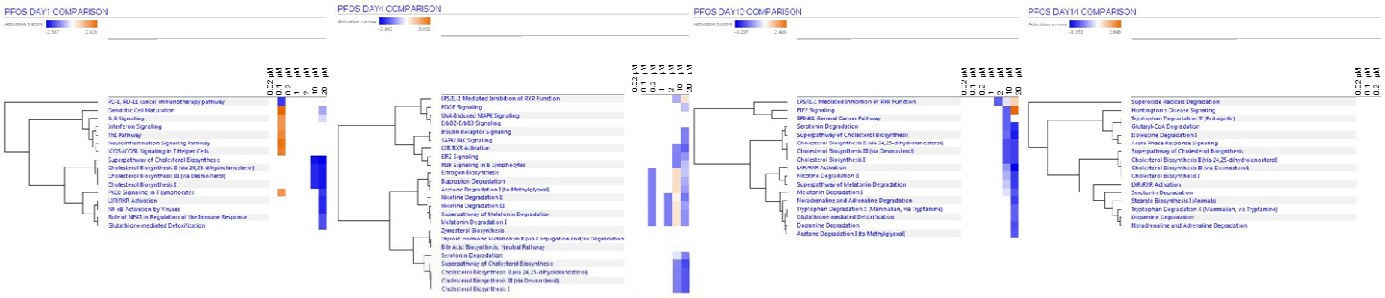

Supplemental File 4. Pathway enrichment for all concentrations of PFOS over time points are shown as an example of how pathway enrichment increased with concentration. Filters for this analysis were set to z-score = to 2.0 and Benjamini–Hochberg adjusted p-value = 0.05. Blue represents inhibited pathways and orange represents activated pathways.

	Day	BMD (95 % CI)
PFBS	1	54.9 (51.8, 61.7)
PFOA	1	38.9 (39.1, 46.0)
PFOS	1	7.3 (59.9, 76.5)
PFDS	1	18.8 (63.3, 78.1)
PFBS	4	73.9 (15.2, 24.8)
PFOA	4	54.4 (8.20, 13.0)
PFOS	4	6.2 (4.8, 11.6)
PFDS	4	7.4 (6.2, 8.4)
PFBS	10	43.2 (34.7, 42.3)
PFOA	10	28.8 (27.0, 31.0)
PFOS	10	6.7 (4.10, 7.4)
PFDS	10	10.0 (51.9, 57.1)
PFBS	14	63.7 (6.5, 8.3)
PFOA	14	5.6 (5.9, 7.4)
PFOS	14	7.3 (6.8, 8.2)
PFDS	14	7.6 (4.6, 7.0)

Supplemental File 5. Overall BMCs (95 % CI) by Day